# Rotorcraft simulations using a sliding-grid approach

**O.J. Boelens› H. van der Ven, J.C. Kok and B.B. Prananta**
National Aerospace Laboratory NLR
Anthony Fokkerweg 2, 1059 CM, Amsterdam, The Netherlands
e-mail: boelens@nlr.nl, venvd@nlr.nl, jkok@nlr.nl, prant@nlr.nl

**Key words:** CFD, sliding grid, GOAHEAD, NICETRIP

**Abstract:** In recent years the National Aerospace Laboratory NLR has participated in several EU-funded helicopter projects, such as GOAHEAD and NICETRIP. In the framework of these projects a sliding-grid approach has been developed in order to more realistically simulate the flow around a complete helicopter. This sliding-grid approach is demonstrated for a tilt-rotor/wing conversion test case performed during the EU-project NICETRIP. Good agreement with experimental data has been obtained. It has been demonstrated that the sliding grid approach is capable of accurately simulating the vortex convection through an interface. Finally, some remarks are made on how the sliding-grid approach will be applied during the post test phase of the EU-project GOAHEAD.

## 1. INTRODUCTION

An important topic during helicopter development is the level of vibration in the cabin. These vibrations can be detrimental to the structure and hampering to the crew. They originate from many sources, one being the interaction of the (vortical) flow around the helicopter with the rotor blades and/or fuselage (for example during tail shake). The rotor-induced vibrations are passed through the rotor driving mechanism and fuselage to the cabin. High vibration levels limit the range of operational use of helicopters severely. In addition, these interactions are responsible for the typical helicopter noise. Especially during low-speed descent, the interaction of the tip vortices and the rotor blades (Blade Vortex Interaction) causes strong pressure fluctuations on the blades and associated high noise levels.

Accurate and efficient simulation of the vortex-dominated flow around helicopters still poses a major challenge. This fact impedes the routinely-based application of such simulations in the research of helicopter noise and vibration.

In recent years the National Aerospace Laboratory NLR has participated in several EU-funded helicopter projects, such as GOAHEAD [1] and NICETRIP [2]. The present paper discusses work performed in the framework of these projects to increase the technology readiness of the methods used at NLR to simulate the flow around rotorcraft. First the methods available at NLR and their application during the blind test phase of the EU-project GOAHEAD will be discussed. Next, the sliding-grid approach developed at NLR will be discussed. The approach will be demonstrated for a tilt-rotor/wing conversion test case performed during the EU-project NICETRIP. The paper concludes with some remarks on how the sliding-grid approach will be used during the post test phase of the EU-project GOAHEAD.

### 1.1 Methods used for helicopter CFD simulations available at NLR

At the National Aerospace Laboratory NLR three methods are used for simulation of the flow around rotorcraft. Each of these methods will be discussed briefly in the following sections.

### 1.1.1 Discontinuous Galerkin finite element method

The discontinuous Galerkin finite element method solves the compressible Euler equations of gas dynamics in an arbitrary Lagrangian-Eulerian formulation to accommodate moving meshes. Details of the flow solver can be found in [3] and [4].

Of particular relevance for the simulation of vortex dominated flows is the fact that the Discontinuous Galerkin method not only solves for cell-averaged flow data, but also for the flow gradients. The flow gradients are used to determine the vorticity directly and as such vorticity transport is contained in the discrete equations. Moreover, the Discontinuous Galerkin method is ideally suited for local grid refinement.

### 1.1.2 Discontinuous Galerkin multi-time multi-grid method

The basic idea of the multi-time multi-grid algorithm [5] is that a time-periodic problem can be considered a steady problem in the sense that after one time period the next period shows the same physical phenomena. This is formalized by solving the time-dependent equations simultaneously in both space and time for the complete period of the problem. This is contrary to the usual time-serial approach, where one proceeds time step after time step on spatial grids. Now the time-dependent equations are solved on a four-dimensional space-time grid which contains all time levels in a period. Apart from generating a periodic solution by construction, the most relevant advantage for rotor simulations is that the time-accurate coupling of different physics models is straightforward.

The current algorithm contains four modules, an aerodynamic module for the solution of the flow equations, a mesh refinement module to improve vortex resolution in the flow domain, an elastic module to account for the elastic blade deformations, and a trim module to trim the rotor system.

### 1.1.3 ENSOLV

The flow solver ENSOLV [6], which is part of NLR's flow simulation system ENFLOW [7], is capable of solving the Euler and Navier-Stokes equations on multi-block structured grids for arbitrary configurations. These configurations can be either fixed or moving relative to an inertial reference frame, and can be either rigid or flexible. The equations in full conservation form are discretized in space by a second-order accurate, cell-centred, finite-volume method, central differences and matrix artificial diffusion. The artificial diffusion consists of a blending of second-order and fourth-order differences with a Jameson-type shock sensor for the basic flow equations.

For steady-state simulation, the discretized time-dependent system of equations is integrated toward the steady-state solution using a five-stage explicit Runge-Kutta scheme. Local-time stepping, implicit residual averaging and multi-grid acceleration techniques are applied. For time-accurate simulations, the flow solver uses the dual-time stepping scheme, where for each time-step the time-dependent flow equations are integrated in pseudo-time toward a steady-state solution in a similar way as in the steady flow simulation using the same acceleration techniques.

For helicopter applications a steady actuator disc boundary condition is available to mimic the effect of the rotor.

## 1.2 Helicopter simulations during blind test phase of the EU-project GOAHEAD

During the blind test phase of the EU-project GOAHEAD (Contract Nr. 516074) [1] NLR has performed steady-state Navier-Stokes simulations (using the Turbulent Non-Turbulent (TNT) k-ω turbulence model [8]) for the GOAHEAD helicopter configuration employing the CFD flow solver ENSOLV [6]. The case considered was a high-speed tail-shake condition [1] [2]. The effect of the main and tail rotor was modelled by means of steady actuator discs.

The input data for the main rotor actuator disc was obtained from a Discontinuous Galerkin multi-time multi-grid Euler simulation (see section 1.1.2) for the isolated main rotor. The rotor was trimmed to the prescribed thrust and zero rotor moments. Elastic blade deformations were included in this simulation. No grid adaptation was performed. For the tail rotor a constant-thrust actuator disc was used.

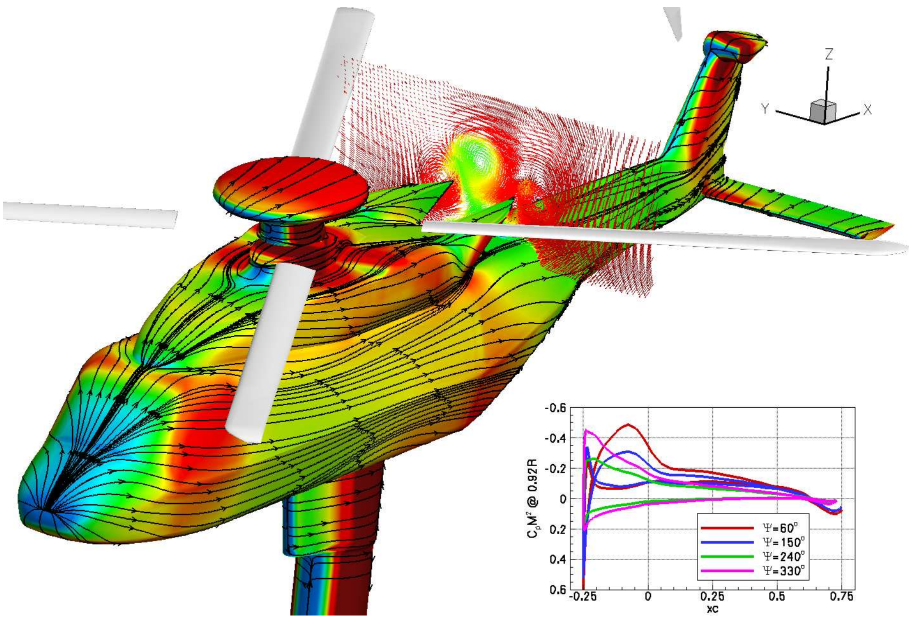


Figure 1: Result obtained for the high-speed tail-shake test case during the blind-test phase of the EU-project GOAHEAD. The rotors are modeled by means of steady actuator discs. The instantaneous Mach-scaled pressure coefficient on the blade section is obtained using the Discontinuous Galerkin multi-time multi-grid method. The pressure coefficient on the fuselage, the skin friction lines and the velocity field data are obtained using ENSOLV.

Although giving satisfactory results (see [9] and Figure 1), the used steady-state approach lacks the full unsteadiness of the rotor induced flow field as well as the proper interaction between the rotor and the fuselage, needed for noise and vibration investigations.

# 2. SLIDING-GRID APPROACH

In order to simulate the flow around a helicopter more realistically, a sliding-grid approach has been developed at NLR. In this approach two grids are used, one about the rotating part and one about the fixed part. The grids connect at planar and cylindrical interfaces in a non-overlapping way. The grid lines across the interface are not aligned. In order to simulate the rotor rotation, the grid about the rotating part rotates within the grid about the fixed part in such a way that the interfaces remain planar and cylindrical.

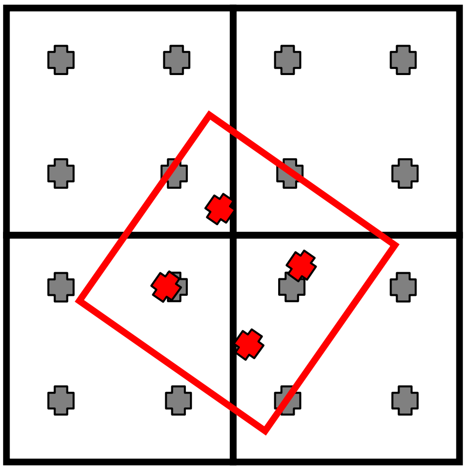

Figure 2: The interpolation problem on the interface (in case of the Discontinuous Galerkin method). The red face connected to a cell in the grid about the rotating part is arbitrarily oriented with respect to the black faces connected to the grid about the fixed part. In the red cell four Gauss quadrature points are shown to which the solution in the gray points should be interpolated.

The interface is treated as an internal boundary, so flow states between neighbouring cells need to be exchanged across the interface. Since the grids at the moving interface are not aligned, the required flow state information is not readily available at each side of the interface. Therefore the flow states in the interface are interpolated to the desired locations. See Figure 2 for an illustration.

The interpolation is performed by a volume spline method. For more details on the volume spline method used see [10].

## 3. DEMONSTRATION OF SLIDING GRID APPROACH

### 3.1 Description of test case

The sliding grid approach has been demonstrated for a planar interface within the EU-project NICETRIP (Contract Nr. 030944) [2] employing the Discontinuous Galerkin finite-element method (see section 1.1.1). The test concerns test TP4 of the EU—project TILTAERO wind tunnel test campaign, which is a tilt-rotor/wing conversion case, see Figure 3. The wind tunnel test conditions are shown in Table 1.

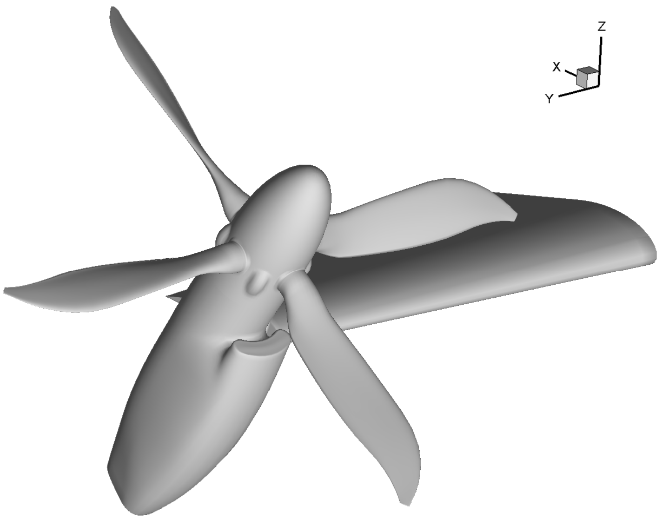

Figure 3: TILTAERO tilt-rotor/ wing conversion TP4 configuration.

In the simulation the commanded control angles have been used. The commanded control angles differed significantly (up to 2.4° for the lateral cyclic) from the measured control angles. The gimbal motion has been ignored in the simulation. The angle between the fixed and moveable wing (0.7°) has been set to zero. The angle between the moveable wing and the nacelle has been set to 56.3°, consistent with the experiment.

| | |
|---|---|
| Speed [m/s] | 57.1 |
| Speed of sound [m/s] | 338.3 |
| Rotor speed [RPM] | 1107.0 |
| Nacelle angle (relative to fixed wing) [°] | 57.0 |
| Fixed wing angle of attack (relative to air stream) [°] | 3.0 |
| Movable wing pitch (relative to fixed wing) [°] | 0.7 |

Table 1: Wind tunnel test conditions for TILTAERO TP4.

### 3.2 Computational grid

For the present case the grids about the rotating part and about the fixed part are only connected at a planar interface. No cylindrical interface is present. The two grids have been generated using the grid generation tools of NLR's flow simulation system ENFLOW [7]. The grid about the fixed part has been generated using the Cartesian grid mapping technique developed at NLR [11].

Details of the two computational grids connected through the sliding interface are shown in Figure 4 and Figure 5. In these figures the grid about the rotor is shown in blue, whereas the grid about the fixed wing is shown in orange.

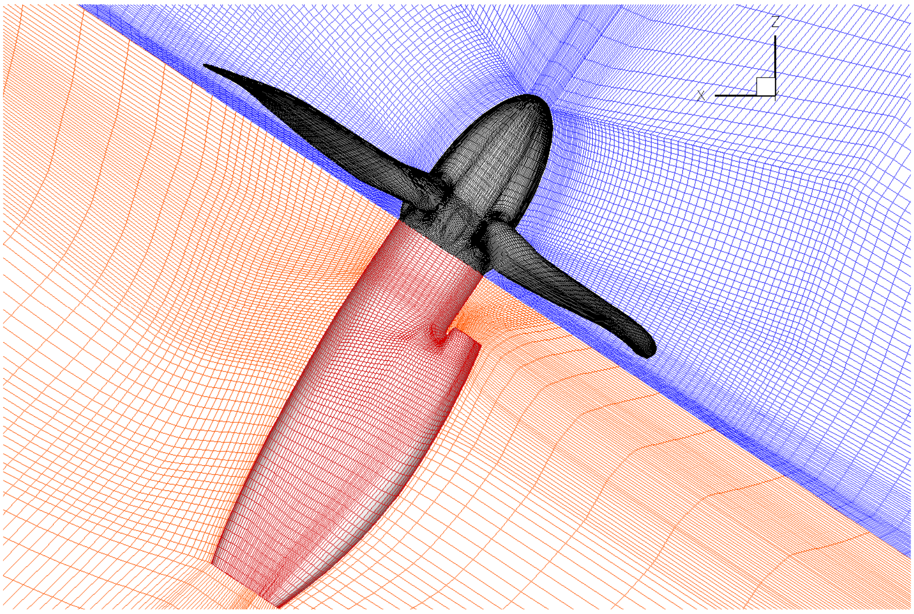

Figure 4: Side view of the computational grids. The grid about the wing is shown in orange, the grid about the rotor is shown in blue.

Figure 4 shows a side view, such that the rotor and nacelle are visible. This figure shows that the interface is quite close to the rotor blades.

Figure 5 shows the interface grid both for the grid about the rotor and the grid about the fixed wing. The interface grids are quite different, which is caused by the geometrical constraints. Note that not only the face orientation is different for the grids, but that also the resolution varies significantly.

The simulation has been performed on a one-level coarser grid than the grid shown in the figures.

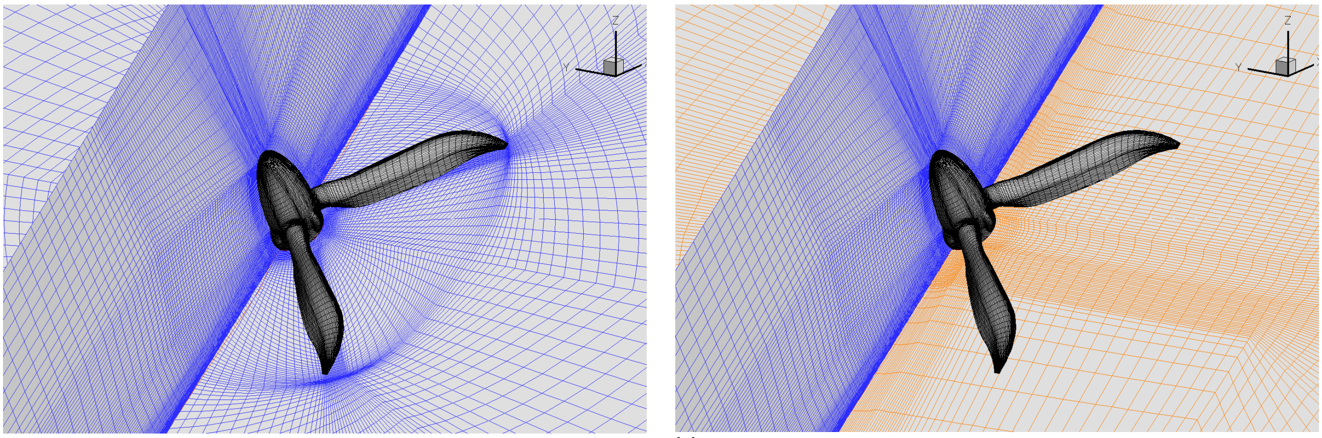

a) b)

Figure 5: a) Sliding grid interface of the grid about the rotor. The blades and spinner are shown in black, the interface in blue. b) Sliding grid interface of the grid about the fixed wing grid. The blades and spinner are shown in black, the wing interface grid in orange.
For both figures a cross-sectional plane through the rotor grid is shown in blue.

The grid about the fixed wing has been pre-adapted in the expected vortex regions to improve the grid resolution near the interface. The aim of the pre-adaptation was to have comparable grid resolution at both sides of the interface at the instances when the tip vortex emanating from the blade at 270° azimuthal angle[1] passes through the interface. The resulting grid used during the simulations is shown in Figure 9.

The grid about the rotor contains approximately 250.000 cells, whereas the grid about the fixed wing contains approximately 300.000 cells.

The pitch schedule is accommodated in one cell layer near the blade root, i.e. the blades move with the commanded pitch schedule, the nacelle rotates in a rigid way, and the difference in motion is overcome in one cell layer near the blade root.

The interpolation on the sliding grid interface is based on the ten nearest neighbours [10].

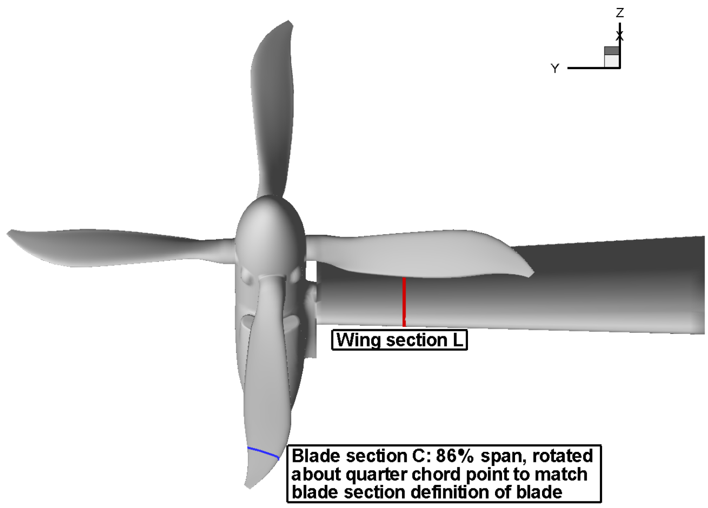


Figure 6: Location of blade section C (86% span) and wing section L.

### 3.3 Results

The simulation has run for four rotor revolutions. Each revolution can be subdivided into four periods. In the simulation each period has been subdivided into thirty-two time steps. For a conventional scheme this corresponds to a temporal resolution of about 1.4° azimuth angle. Blade data will be presented for the last period, whereas wing data will be presented for the last full rotor revolution.

[1] Zero azimuthal angle $\psi=0°$ is defined as the position with the blade pointing upward when the tilt rotor is in propeller model.

### 3.3.1 Definition of blade and wing sections

The blade and wing sections for which unsteady pressure data will be compared are shown in Figure 6.

### 3.3.2 Pressure distribution at blade section C

The time-dependent pressure distribution at blade section C is shown in Figure 7. For twelve azimuthal positions at 30° intervals the Mach-scaled pressure coefficient (the reference velocity is the free stream speed of sound) is presented.

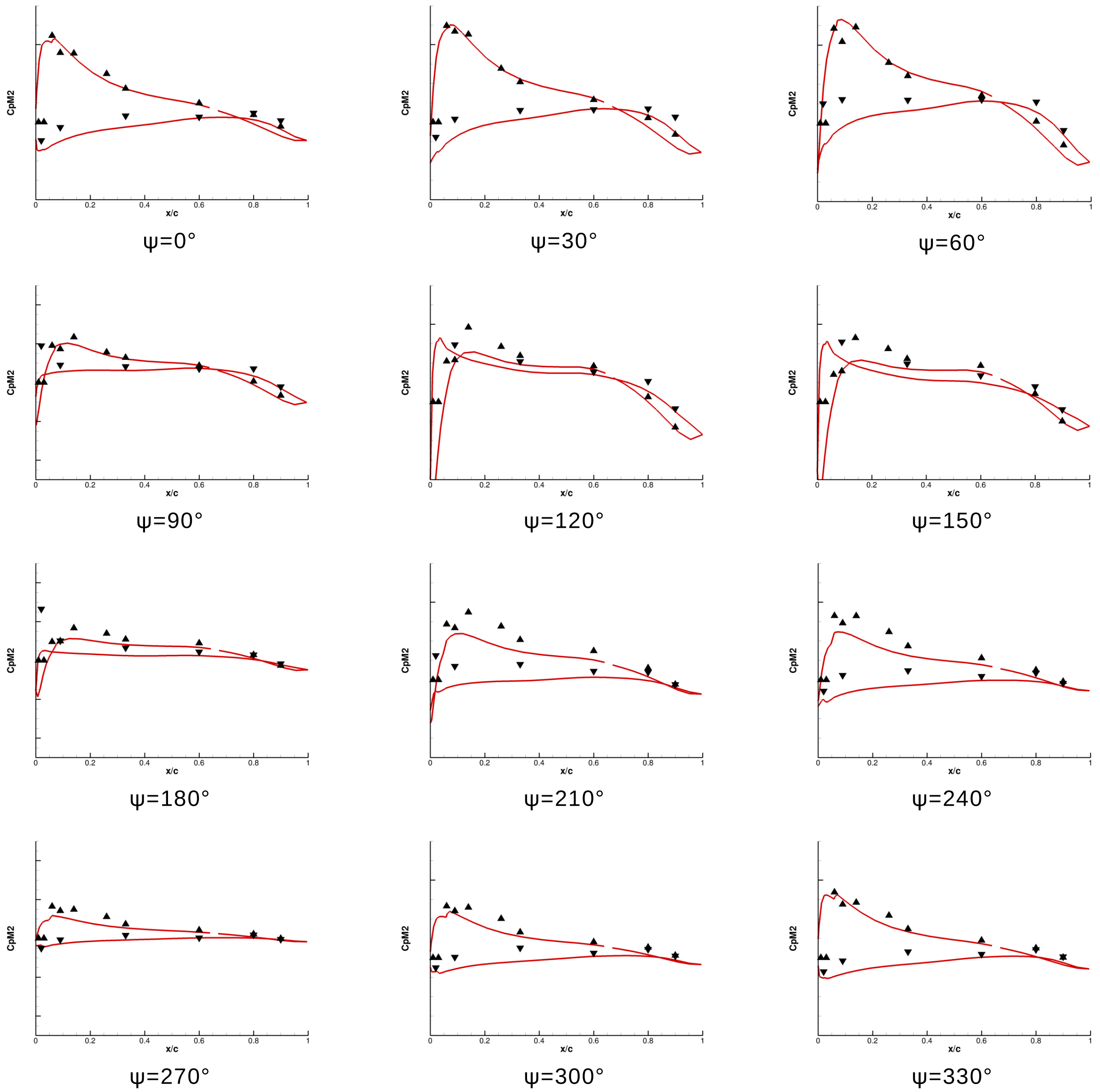


Figure 7: Instantaneous Mach-scaled pressure coefficient at blade section C as function of different azimuth angles. Solid red lines are the results of the simulation, symbols are the experimental data (delta symbols for the upper side, gradient symbols for the lower side).

The general agreement in shape of the pressure profiles is good considering the uncertainty in the pitch schedule and the inviscid modelling.

### 3.3.3 Time history of fluctuating part of the pressure in wing section L

The time history of the fluctuating part of the pressure (mean pressure is subtracted from the pressure signal) at two points on wing section L (78% wing span) is shown in Figure 8. The points are located at 2.3% wing chord on the lower side of the wing and 2.9% wing chord on the upper side of the wing. The time has been transformed to the azimuth angle ψ of one of the blades. The 4/rev oscillation corresponds to the blade passing frequency, i.e. the vortex impingement on the wing.

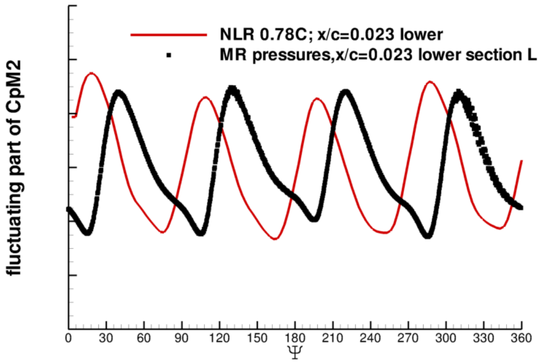


a)

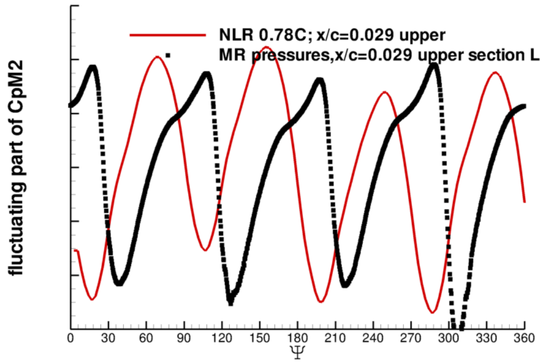


b)

Figure 8: a) Fluctuating part of the unsteady Mach-scaled pressure coefficient at 2.3% wing chord on the lower side of wing section L (78% wing span). b) Fluctuating part of the unsteady Mach-scaled pressure coefficient at 2.9% wing chord on the upper side of wing section L (78% wing span). Solid red lines are the results of the simulation, symbols are the experimental data.

Apparent from this figure, the agreement in the amplitude of the fluctuations is good, whereas a phase difference between the simulation and the experiment of about 30 degrees exists. There can be a number of reasons for this phase shift. The exact location of the tip vortex critically depends on the blade motion, gimbal motion and wing deformation. Each of these factors is either not know in sufficient detail from the experiment or differs between the experiment and the simulations.

### 3.3.4 Details of the simulated flow

The capability of the sliding interface to allow passage of a tip vortex is examined in Figure 9. This figure shows the grid and the vorticity magnitude in a cross-section at 65% wing span. In Figure 9a) corresponding to an azimuthal angle of ψ=253° the tip vortex of the visible blade is still above the interface. In Figure 9b) and Figure 9c) the vortex moves through the interface. In Figure 9d) the vortex has completely passed through the interface. Comparing Figure 9a) and Figure 9d) the vortex has passed through the interface losing little of its strength.

Figure 10 shows the vortical flow around the configuration at ψ=33°. The figure nicely shows the tip vortex emanating from the blade at an azimuthal angle of 303°.

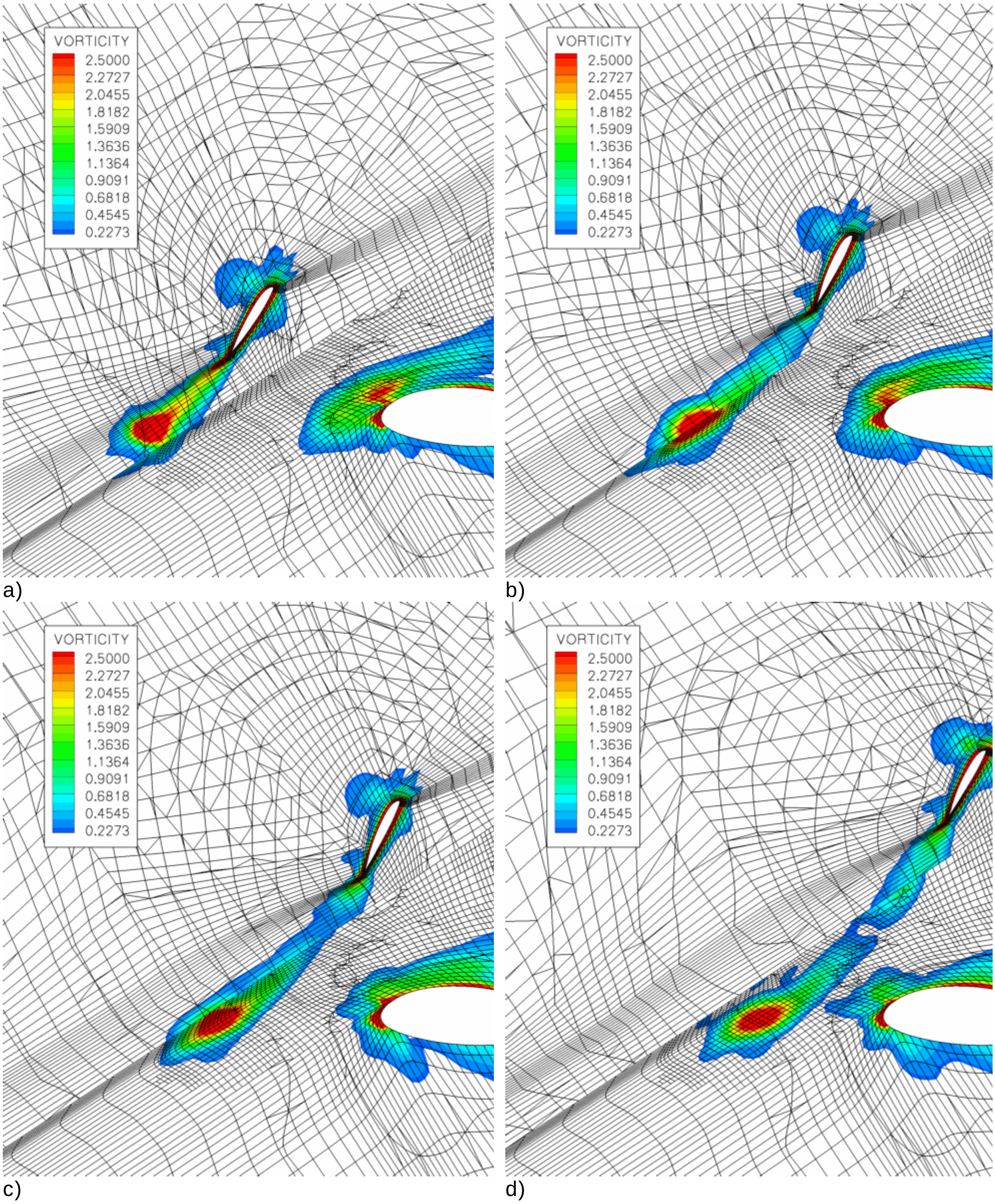


Figure 9: Instantaneous grid and flow features (vorticity magnitude) at 65% wing span. Note the pre-adaptation of the wing grid. a) ψ=253°, the tip vortex of the visible blade is visib le in grid about the rotor. b) ψ=270°, the tip vortex of the visible blade is passi ng through the interface. c) ψ=281°, the tip vortex of the visible blade is passi ng through the sliding grid interface, d) ψ=298°, the tip vortex of the visible blade has succ essfully crossed the sliding grid interface.

The pre-adapted regions in the grid about the wing are essential to correctly capture the vortex convection. In regions with insufficient grid resolution the vortex is dissipated very rapidly, see for example the vortex emanating from the blade at an azimuthal angle of 33° in Figure 10.

### 3.4 Concluding remarks

Through the simulation of a tilt-rotor/wing configuration during conversion it has been demonstrated that the sliding grid approach is capable of accurately simulating the vortex convection through an interface. The grid resolution on both sides of the interface should be comparable to minimize the dissipation of vorticity.
The sliding grid approach, therefore, is a feasible approach for the CFD simulation of interaction phenomena encountered in rotorcraft applications.

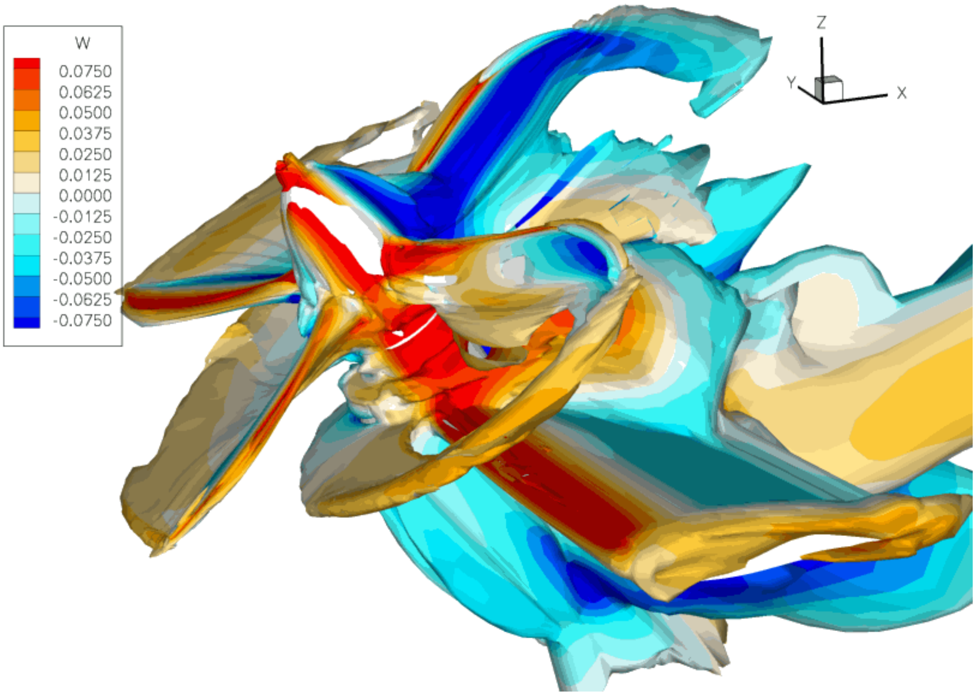


Figure 10: Instantaneous vorticity contour at ψ=33°. The iso-contour is colored using the vertical component of the velocity vector.

## 4. FUTURE ACTIVITIES

### 4.1 Helicopter simulations during post test phase of the EU-project GOAHEAD

The post test phase of the EU-project GOAHEAD [1] will take place during the second half of 2008 and early 2009. During this phase NLR will reconsider the high-speed tail-shake test case. Instead of the steady-state Navier-Stokes simulation performed during the blind test phase the simulation will be a time-accurate Navier-Stokes simulation with both a rotating main and tail rotor. Thus the full unsteadiness of the rotor induced flow field and the proper interaction between the rotor and the fuselage will be simulated. This simulation will be performed employing the CFD flow solver ENSOLV.

### 4.2 Modifications to ENSOLV

As stated in section 1.1.3 during the blind test phase the flow solver ENSOLV was only able to mimic the effect of a rotor by means of a steady actuator disc boundary condition. Since the completion of the blind test phase, the flow solver ENSOLV is augmented with the following functionalities to enable a full helicopter simulation:

- The rotor blade motion for multiple rotating systems (main rotor and tail rotor).

- A sliding-grid capability. The approach is based on a spline interpolation similar to the one used in the Discontinuous Galerkin finite-element method. However, both planar and cylindrical interfaces can be used now. In addition, the nearest neighbour search algorithm has been improved.
- An aeroelastic blade deformation capability. The flow solver ENSOLV has an aeroelastic module which has been frequently used for fixed wing applications. This module has been augmented to include rotating blade deformation.

In addition, the coupling of the flow solver ENSOLV to the aeromechanical code Flightlab [12] for trimming purposes is also under investigation.

These functionalities are presently being tested, so that they can be readily used during the post test simulations of the EU-project GOAHEAD

## ACKNOWLEDGMENTS

This work is partly supported by the European Union under the Integrating and Strengthening the European Research Area Programme of the 6th Framework, Contract NR. 516074 (GOAHEAD project) and Contract Nr. 030944 (NICETRIP project).

## REFERENCES

[1] K. Pahlke, *"The GOAHEAD project"*, 33rd European Rotorcraft Forum, Kazan, Russia, 2007.

[2] "Novel Innovative Competitive Effective Tilt Rotor Integrated Project", URL: http://nicetrip.onera.fr [cite July 2008].

[3] J.J.W. van der Vegt and H. van der Ven, *"Space-time discontinuous Galerkin finite element method with dynamic grid motion for inviscid compressible flows. Part I. General formulation"*, J. of Comp. Physics, 182, 546-585, 2002.

[4] H. van der Ven and O.J. Boelens, *"A framework for aeroelastic simulations of trimmed rotor systems in forward flight"*, 30th European Rotorcraft Forum, Marseille, France, 2004, also available as NLR-TP-2004-409.

[5] H. van der Ven, *"An adaptive multitime multigrid algorithm for time-periodic flow simulations"*, J. of Comp. Physics, 227, 5286-5303, 2008.

[6] J.C. Kok and S.P. Spekreijse, *"Efficient and accurate implementation of the k-ω turbulence model in the NLR multi-block Navier-Stokes system"*, ECCOMOAS 2000, Barcelona, Spain, 11-14 September, 2000, also available as NLR-TP-2000-144.

[7] *"ENFLOW: A computer code system for accurate simulation of three-dimensional flows"*, URL: http://www.nlr.nl/documents/flyers/f222-01.pdf [cited July 2008].

[8] J.C. Kok, *"Resolving the dependence on free-stream values for the k-ω turbulence model"*, NLR-TP-99295, 1999.

[9] O.J. Boelens et al., *"The blind-test activity of the GOAHEAD project"*, 33rd European Rotorcraft Forum, Kazan, Russia, 2007.

[10] M.H.L. Hounjet and J.J. Meijer, *"Evaluation of Elastomechanical Aerodynamic Data Transfer Methods for non-planar Configurations in Computational Aeroelastic Analysis"*, In Proceedings of 1995 CEAS International Forum on Aeroelasticity and Structural Dynamics, Jun Manchester, 1995, also NLR-TP-95690, NLR, 1995.

[11] O.J. Boelens, S.P. Spekreijse, H.A. Sytsma and K.M.J. de Cock, *“Comparison of measured and simulated flow features for the full-scale F-16XL aircraft”*, NLR-TP-2007-264, 2007.

[12] Advanced Rotorcraft Technology, Mountain View, Flightlab ™